

# Synthesis and Search for Design Principles of New Electron Accepting Polymers for All-Polymer Solar Cells

In Hwan Jung,<sup>†</sup> Wai-Yip Lo,<sup>†</sup> Jaeyoung Jang,<sup>†</sup> Wei Chen,<sup>‡</sup> Donglin Zhao,<sup>†</sup> Erik S. Landry,<sup>‡</sup> Luyao Lu,<sup>†</sup> Dmitri V. Talapin,<sup>†,§</sup> and Luping Yu<sup>\*,†</sup>

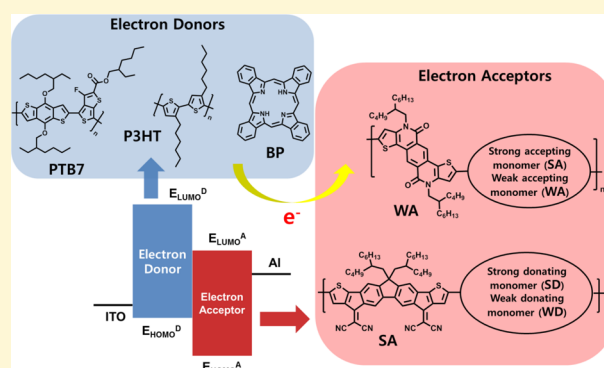
<sup>†</sup>Department of Chemistry and The James Franck Institute, The University of Chicago, Chicago, Illinois 60637, United States

<sup>‡</sup>Materials Science Division, Argonne National Laboratory, Argonne, Illinois 60439, United States

<sup>§</sup>Center for Nanoscale Materials, Argonne National Laboratory, Argonne, Illinois 60439, United States

## Supporting Information

**ABSTRACT:** New electron withdrawing monomers, thieno[2',3':5',6']pyrido[3,4-g]thieno[3,2-c]isoquinoline-5,11(4*H*,10*H*)-dione (TPTI) and fluorenedicyclopentathiophene dimalononitrile (CN), have been developed and used to form 12 alternating polymers having different monomer combinations: (a) weak donating monomer–strong accepting monomer, (b) weak accepting monomer–strong accepting monomer, (c) weak accepting monomer–weak accepting monomer, and (d) strong donating monomer–strong accepting monomer. It was found that lowest unoccupied molecular orbital (LUMO) energy levels of polymers are significantly determined by stronger electron accepting monomers and highest occupied molecular orbital (HOMO) energy levels by the weak electron accepting monomers. In addition, fluorescent quantum yields of the TPTI-based polymers in chloroform solution are significantly decreased as the LUMO energy levels of the TPTI series of polymers become deeper. The quantum yield was found to be closely related with the photovoltaic properties, which reflects the effect of internal polarization on the photovoltaic properties. Only the electron accepting polymers showing SCLC mobility higher than  $10^{-4}$  cm<sup>2</sup>/(V s) exhibited photovoltaic performance in blend films with a donor polymer, and the PTB7:PNPDI (1:1.8 w/w) device exhibited the highest power conversion efficiency of 1.03% ( $V_{oc} = 0.69$  V,  $J_{sc} = -4.13$  mA/cm<sup>2</sup>, FF = 0.36) under AM 1.5G condition, 100 W/cm<sup>2</sup>. We provide a large set of systematic structure–property relationships, which gives new perspectives for the design of electron accepting materials.



## INTRODUCTION

Currently, most popular bulk heterojunction (BHJ) solar cells require the use of fullerene derivatives as the electron acceptor for facile photoinduced electron transfer from electron rich low band gap polymer donors.<sup>1–4</sup> The fullerene derivatives, phenyl-C<sub>61</sub>(or71)-butyric acid methyl ester (PC<sub>61</sub>BM and PC<sub>71</sub>BM), are almost exclusively used as acceptors due to their high electron affinity and electron mobilities. However, these fullerenes are rather expensive and exhibit limited absorption in the longer wavelength region of the solar spectrum and thermal instability in the morphology of blend films.<sup>5–9</sup> There is a question resonating in the community working on polymeric solar cells: can we replace the fullerene with electron-deficient polymers? Although the electron donating polymers have been extensively studied and can generate power conversion efficiency (PCE) over 7% routinely in small area devices in combination with fullerenes,<sup>10–15</sup> it is still challenging to find n-type polymers or organic molecules that rival the electronic properties of fullerenes. Both intellectual curiosity and economical reason lead us to explore new, more cost-effective and efficient

electron accepting materials. For several decades, n-type polymers are extensively studied for use in organic field-effect transistors (FETs) and high electron mobility up to 1 cm<sup>2</sup>/(V·s) has been achieved.<sup>16–22</sup> However, only a few polymers were successfully applied to solar cells.<sup>23–26</sup> The most successful n-type polymer, P(NDI2OD-T2),<sup>27–29</sup> exhibited FET mobility up to 0.85 cm<sup>2</sup>/(V·s)<sup>27</sup> and space charge limited current (SCLC) mobility of  $5 \times 10^{-4}$  cm<sup>2</sup>/(V·s).<sup>30</sup> Recently, diketopyrrolopyrrole-based PDPP2TzT polymer resulted in a PCE of 2.9% with FET mobility up to 0.13 cm<sup>2</sup>/(V·s).<sup>31</sup> The Polyera Corp. disclosed a certified all-polymer photovoltaic cell with a PCE over 6%.<sup>32</sup>

Although the FET mobility of these polymers already surpasses that of fullerene derivatives, there are many other factors that influence the photovoltaic performances. A crude design idea for the electron acceptors is that it must exhibit

Received: March 3, 2014

Revised: May 6, 2014

proper energy levels to match with the electron donor polymers, ideally similar to those of fullerene. Studies from polymer/fullerene BHJ solar cells indicated that the  $E_{\text{LUMO}}^{\text{D}} - E_{\text{LUMO}}^{\text{A}}$  offset should be around 0.3–0.8 eV for efficient photo induced charge transfer at the donor–acceptor interface.<sup>33,34</sup> In addition, the polymers must exhibit the proper absorption bandgap to effectively harvest solar energy. It is also crucial to achieve a nanoscale, bicontinuous, and interpenetrating network of the donor and acceptor phases in order to facilitate charge separation and transport.<sup>35</sup>

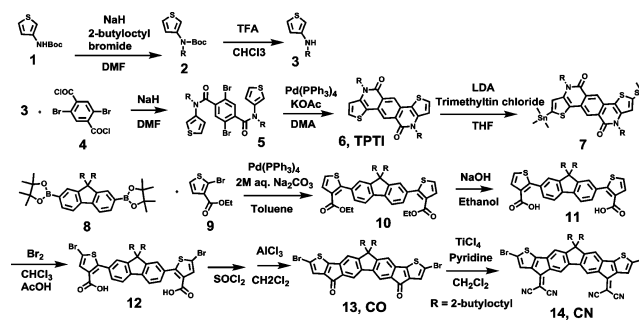
In this work, we attempt to further develop the general design guidelines for synthesizing new electron accepting polymers. A major focus is to figure out how to control and fine-tune the energy levels and electron accepting properties. First, we developed new electron accepting monomers, 4,10-bis(2-butyloctyl)thieno[2',3':5,6]pyrido[3,4-g]thieno[3,2-c]-isoquinoline-5,11-dione (TPTI) and fluorenedicyclopentathio-phenylene dimalononitrile (CN).<sup>36</sup> Based on these new monomers, we have synthesized a series of alternating accepting polymers with the following monomer–co-monomer combination: (a) weak donating monomer–strong accepting monomer (WD-SA), (b) weak accepting monomer–strong accepting monomer (WA-SA), (c) weak accepting monomer–weak accepting monomer (WA-WA), and (d) strong donating monomer–strong accepting monomer (SD-SA). We investigated the physical, optical, and electrochemical properties and the electron transporting and photovoltaic characteristics of the resultant polymers to extract a close relationship between each characteristic and polymer structure. Several criteria for designing electron accepting polymers for all-polymer solar cells are suggested.

## RESULTS

**Synthesis and Structural Characterization.** The initial design strategy to n-type semiconducting polymers involves considerations of the two issues. First of all, we need compounds that can be converted into distannanyl monomers for the Stille polycondensation, which will exclude many electron-deficient compounds whose distannanyl derivatives exhibit a limited reactivity for polymerization. Second, we need to ensure that the energy levels of materials (highest occupied molecular orbital/lowest unoccupied molecular orbital (HOMO/LUMO)) are lowered enough to match with those in donor polymers. The following molecular architectures of accepting polymers were conceived with repeating units: (a) WD-SA, (b) WA-SA, (c) WA-WA, and (d) SD-SA. Those with SA-SA are not pursued here due to the limitation in polymerization. The structures of the new monomers (compounds 6 and 14) designed for these purposes are shown in Scheme 1. Specifically, the new cyclic diamide monomer, TPTI, shows a highly planar structure facilitating intermolecular ordering. The end thiophene structures enable further functionalization at the 2-position of the thiophenes to introduce distannanyl groups (compound 7). The two electron withdrawing carbonyl moieties enhance the electron affinity of the conjugated system, resulting in a weak accepting monomer. The alkyl groups allow tuning of the solubility of the rigid conjugated backbone in organic solvents.

A total of eight dibromo monomers, all electron-deficient, were synthesized and co-polymerized with three distannanyl monomers: monomer 7 (WA), BDT (WD), and EDOT (SD). The CN (compound 14) monomer exhibits strong electron accepting properties and has a rigid conjugated backbone,

Scheme 1. Synthetic Routes to the Synthesized Monomers



facilitating efficient  $\pi$ -electron delocalization and intermolecular order. To enhance the solubility of the resulting polymers, a fluorene moiety with the two alkyl side chains at the C-9 position is introduced.

The synthetic approaches to the two new monomers are outlined in Scheme 1, and their detailed synthetic procedure is described in the Supporting Information (SI). Starting from the commercially available *N*-Boc-3-aminothiophene, compound 2 was synthesized by alkylation with 2-butyloctyl bromide using sodium hydride. The Boc functional group in compound 2 was easily deprotected by trifluoroacetic acid (TFA) to afford compound 3. Without further purification, compound 3 was reacted with acid chloride 4, generated in situ from the reaction of 2,5-dibromoterephthalic acid with thionyl chloride, to give the amide compound 5. Direct intramolecular arylation of compound 5 was performed via C–H bond activation with KOAc as the base and Pd(PPh<sub>3</sub>)<sub>4</sub> as the catalyst at 120 °C in dimethylacetamide (DMA). Under diluted condition (2 mM), the arylation of compound 5 was completed within 6 h to generate compound 6 with a yield higher than 80%. The final monomer 7 was synthesized by stannylation with trimethyltin chloride after lithiation of compound 6 with lithium diisopropylamide (LDA) at –78 °C. The 2,2'-(9,9-bis(2-butyloctyl)-9*H*-fluorene-2,7-diyl)dithiophene-3-carboxylic acid (11) was synthesized according to the literature.<sup>37</sup> Bromination of compound 11 with bromine under acid condition yielded compound 12. The carboxylic acid of compound 12 was converted into acyl chloride using thionyl chloride, which was converted into compound 13 via intramolecular acylation.

The introduction of bromo functionality into the 2 and 2' positions of compound 12 prevented intermolecular acylation of compound 12, resulting in compound 13 (>80%). Compound 14 (CN) was synthesized by Knoevenagel condensation using malononitrile and TiCl<sub>4</sub> under basic condition. Monomer 13 (CO) containing a carbonyl group exhibits weaker electron withdrawing property than monomer 14 (CN). EDOT is a stronger electron donating moiety than BDT. Through the combination between two electron donating monomers (EDOT and BDT) and two electron accepting monomers (CO and CN), four kinds of D–A alternating copolymers (PBCO, PBCN, PECO, and PECN) were synthesized.

SW and TPD have similar molecular structure. The TPD unit has an electron withdrawing imide group, while SW has a stronger electron withdrawing sulfonimide unit. NDI and PDI are well-known electron accepting units containing diimide functionality. SF, BT, and NT have electron-deficient disulfone, thiadiazole, and dinitro groups, respectively. By combining these electron-accepting co-monomers (TPD, SW, SF, BT, NT,

Scheme 2. Synthetic Scheme for the Electron Accepting Polymer

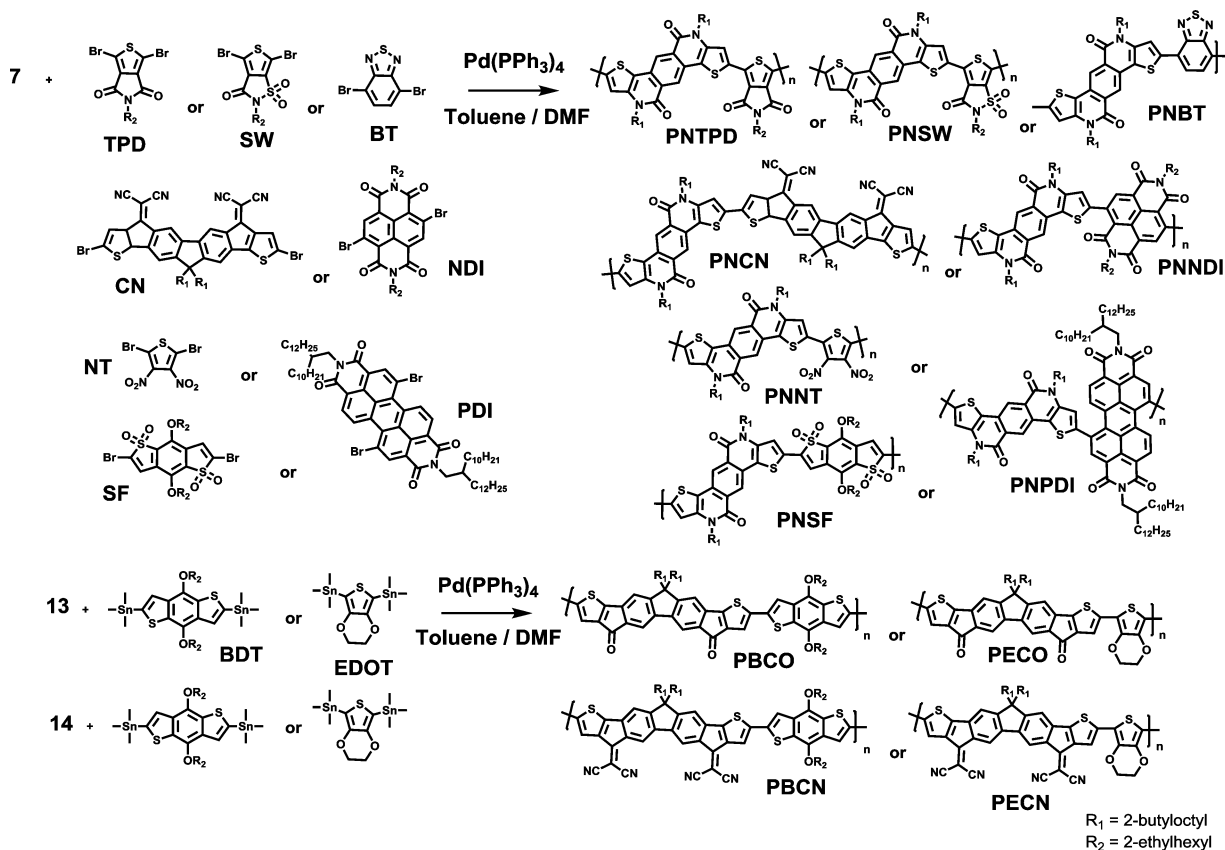


Table 1. Physical Properties of the Polymers

	PNPDI	PNNDI	PNSF	PNSW	PNCN	PNBT	PNNT	PNTPD	PBCO	PBCN	PECO	PECN
$M_r^a$	1720	1147	1167	958	1474	793	831	922	1161	1257	857	953
$M_n^b$	18 100	21 800	16 300	11 500	28 800	15 700	13 600	10 900	13 200	14 400	18 700	21 700
$M_w^c$	39 200	49 400	28 800	18 500	55 100	38 700	25 200	18 000	28 700	40 600	43 100	52 900
PDI	2.17	2.27	1.77	1.61	1.91	2.46	1.86	1.65	2.18	2.81	2.31	2.43
$T_d^d$ , °C	387	331	353	420	358	423	339	409	382	368	381	363

<sup>a</sup>Molecular weight of repeating unit. <sup>b</sup>Number-average molecular weight. <sup>c</sup>Weight-average molecular weight. <sup>d</sup>Decomposition temperature determined by TGA under N<sub>2</sub> based on a 5% weight loss.

NDI, CN, and PDI) with the new cyclic amide monomer 7, eight TPTI-based electron accepting polymers having varied electron withdrawing strengths were synthesized.

The detailed synthetic routes and structures of the final polymers are shown in Scheme 2. The number-average molecular weights ( $M_n$ ) of the resulting polymers, determined by gel permeation chromatography (GPC) with polystyrene as standard, are shown in Table 1. It was found that the TPTI-based polymers exhibited excellent solubility in common organic solvents (i.e., THF, dichloromethane, chloroform, chlorobenzene, and dichlorobenzene). On the other hand, PBCO, PBCN, PECO, and PECN polymers only dissolve in a limited number of organic solvents (i.e., chloroform, chlorobenzene, and dichlorobenzene). The thermal stabilities of the polymers were evaluated by thermogravimetric analysis (TGA) under N<sub>2</sub> atmosphere. All polymers exhibited good stability, showing less than 5% weight loss up to 331–420 °C (Figure S10, SI).

**Polymer Backbone Structure.** The ground-state ( $S_0$ ) geometric structure of the monomers and the four repeating units of the synthesized polymers were optimized with density

functional theory (DFT) using the B3LYP functional and a 6-31G\* basis set.<sup>38–40</sup> The calculated structures of the compounds are shown in Figure S11 (SI), and the dihedral angles at the junction of two monomers in the polymer backbones are summarized in Table 2. The new electron accepting monomers, TPTI and CN, exhibited completely planar backbone structures, facilitating intermolecular ordering in the film state. CO- and CN-based polymers showed a planar polymer backbone with dihedral angle less than 10° due to the small steric hindrance between two thiophene units at the bonding sites of two monomers. However, PNSF and PNSW containing sulfone functionality exhibited a twisted structure with dihedral angle of ~20° due to the bulky sulfone functionality. PNNT containing bulky dinitro thiophene units also showed distorted backbone structure similar to the sulfone-based polymers. PNPDI exhibited a highly distorted backbone structure with a dihedral angle of 48° due to the strong steric hindrance between two hydrogens at the bonding site of TPTI and PDI units. Although it was pointed out that all of the polymers twisted up to about 40° should not have much influence on the polymer conjugation,<sup>41</sup> the twisted polymer

Table 2. Optical Properties and Mobilities of the Polymers

	$\lambda_{\text{abs, sol}} \text{ (nm)}^a$	$\mu_{\text{conf}} \text{ (L/mol}\cdot\text{cm)}^b$	$\lambda_{\text{abs, film}} \text{ (nm)}^c$	$E_{\text{g, opt}}^d$	$\lambda_{\text{em, sol}} \text{ (nm)}^e$	$\text{QY}^e$	$\lambda_{\text{em, film}} \text{ (nm)}^c$	dihedral angle (deg) <sup>f</sup>	FET ( $\text{cm}^2/(\text{V}\cdot\text{s})$ ) <sup>g</sup>	
									n-type	p-type
PBCN	478	110 800	491		530, 574	0.03		7.6	$(1.8-2.8) \times 10^{-5}$	$1.2 \times 10^{-6}$
PBCO	453	81 700	443		644	0.08	677	5.2	$(1.5-2.3) \times 10^{-5}$	$1.7 \times 10^{-8}$
PECN	486, 518, 760	75 100	486, 516, 760		533, 571	0.02		2.4	$(1.3-1.7) \times 10^{-4}$	$(2.7-3.4) \times 10^{-4}$
PECO	472, 734	51 700	460		727	0.05	716	1.7	$(6.2-8.2) \times 10^{-5}$	$2.6 \times 10^{-6}$
PNBT	399, 585	30 500	402, 587	1.63	649	5.83	761	4.4	$(5.6-6.4) \times 10^{-4}$	$5.5 \times 10^{-5}$
PNNNT	535	35 200	576	1.81	660	0.51	704	13.2	$(1.5-2.0) \times 10^{-4}$	$3.2 \times 10^{-5}$
PNTPD	463, 570, 617	43 300	575, 626	1.88	576, 646	8.85	659	1.2	$(6.8-8.0) \times 10^{-4}$	$2.9 \times 10^{-5}$
PNSW	454, 576, 625	39 700	454, 581, 633	1.83	658	6.41	666	26.7	$(3.1-4.1) \times 10^{-4}$	$1.1 \times 10^{-4}$
PNSF	391, 620	50 900	409, 611	1.61	663	1.83	760	21.4	$(1.5-2.3) \times 10^{-3}$	$1.8 \times 10^{-5}$
PNCN	499, 531	93 400	500, 532		581, 641	0.04		16.2	$(7.1-7.9) \times 10^{-4}$	$2.2 \times 10^{-5}$
PNNNDI	395, 658	31 700	422, 660	1.59	787	0.11	801	36.3	$(6.4-9.0) \times 10^{-4}$	$1.6 \times 10^{-4}$
PNPDI	408, 507, 622	53 700	413, 509, 652	1.56	786	0.06	801	47.8		$2.5 \times 10^{-4}$

<sup>a</sup>Dilute solution in chloroform. <sup>b</sup>Molar absorption coefficients from the absorption maximum in diluted solution ( $(5 \pm 0.1) \times 10^{-6}$  M). <sup>c</sup>Spin-cast film on quartz plate from 1 wt % chloroform solution for 30 s at 1500 rpm. <sup>d</sup>Band gap calculated from the absorption edge in solid film. <sup>e</sup>Relative fluorescence quantum yield calculated from QY of the fluorescein in ethanol (0.79). <sup>f</sup>Dihedral angle between two monomers in the polymer backbones calculated from the DFT methods using the GAUSSIAN program. <sup>g</sup>Data from four devices. <sup>h</sup>Average value of the two devices.

structures do affect the molecular ordering in the film states, and thus, charge transport behaviors.

**Optical Properties.** The UV-vis absorption and photoluminescence (PL) emission spectra of the polymers in chloroform (CF) and in films are shown in SI (Figures S14 and S15) and summarized in Table 2. The synthesized polymers exhibited broad absorption covering the entire visible region. The optical bandgap of polymers, estimated by measuring the absorption edge in UV-vis absorption spectra in films, was increased in the following order: PNPDI (1.56 eV) < PNNNDI (1.59 eV) < PNSF (1.61 eV) < PNBT (1.63 eV) < PNNT (1.81 eV) < PNSW (1.83 eV) < PNTPD (1.88 eV).

The CN-based polymers (PBCN, PECN, and PNCN) exhibited more red-shifted absorption maxima with a longer wavelength absorption tail than CO-based polymers (PBCO and PECO) since the dicyanovinyl group is a much stronger electron withdrawing moiety than the carbonyl unit.

In a diluted chloroform solution of equal concentration (concentration,  $5 \pm 0.1 \times 10^{-6}$  M, based on the repeating units of the polymers), the molar absorption coefficients of polymers were determined from the absorption maxima. Polymers PNCN, PBCN, and PECN exhibited much higher molar absorption coefficients due to the highly extended conjugated backbone of the CN monomer. All polymers exhibited molar absorption coefficients over 30,000 L/(mol·cm).

PL emissions of these polymers were measured in solution with excitation at the wavelength of maximum absorption except for the solutions of polymers PNTPD, PNSW, PNSF, PNBT, PNPDI, and PNNNDI, whose emission spectra are largely overlapped with their absorption in solution. These solutions were excited at the wavelengths of 463, 454, 545, 545, 622, and 658 nm, respectively. Most of the polymers exhibited red-shifted emission in the film compared to those in solution due to the enhanced intermolecular  $\pi$ - $\pi$  stacking in the film state. However, the emission of PNPDI and PNNNDI is almost similar both in solution and in the film state due to the highly twisted backbone structures of the two polymers preventing them from intermolecular interaction in the film states.

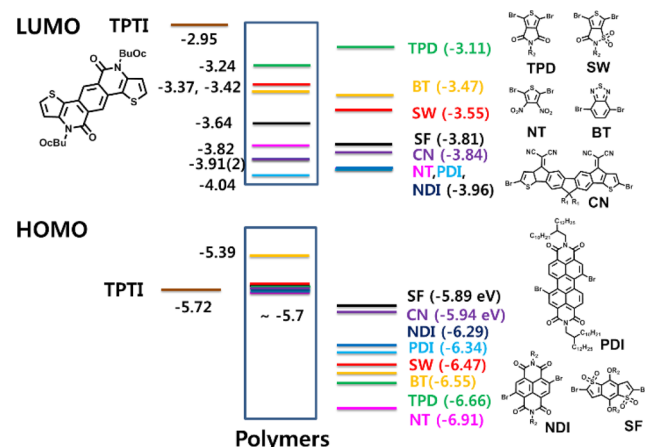
**Electrochemical Properties.** The electrochemical properties of the synthesized monomers and polymers were investigated by using cyclic voltammetry (CV) and summarized in Table 3. The cyclic voltammograms are shown in SI (Figures S16 and S17). The HOMO and the LUMO energy levels of the monomers and polymers were calculated from the oxidation and reduction onset potentials relative to ferrocene (as an internal standard).<sup>42,43</sup> The general trend is that LUMO energy levels of monomers was increased in the order of PDI, NDI (functionality: diimide), and NT (nitro) < CN (dicyano) < SF (disulfone) < SW (sulfonimide) < BT (benzothiadiazole) < CO (dicarbonyl) < TPD (imide) < TPTI (diamide). The diimide functionality is a much stronger electron withdrawing unit than imide, resulting in lower LUMO energy levels of PDI and NDI (−3.96 eV) than that of TPD (−3.11 eV). Since the sulfone functionality is a stronger electron accepting unit than the imide moiety, the LUMO energy level of SW bearing a sulfonimide unit was lower than that of TPD having an imide unit. SF having more sulfone units exhibits a lower LUMO energy level than SW. The new diamide monomer, TPTI, exhibited relatively higher LUMO energy levels of −2.95 eV than TPD having an imide group, thus a weak electron accepting monomer. The LUMO energy level of CN (−3.84 eV) was lower than those of CO and SF monomers.

Table 3. Electrochemical Properties of the Polymers and Monomers

polymers	P-doping (V vs Ag/Ag <sup>+</sup> )		N-doping (V vs Ag/Ag <sup>+</sup> )		$E_g^c$	monomers	P-doping (V vs Ag/Ag <sup>+</sup> )		N-doping (V vs Ag/Ag <sup>+</sup> )		$E_g^c$
	$E_{ox/onset}$	$E_{HOMO}^a$ (eV)	$E_{red/onset}$	$E_{LUMO}^b$ (eV)			$E_{ox/onset}$	$E_{HOMO}^a$ (eV)	$E_{red/onset}$	$E_{LUMO}^b$ (eV)	
PBCN	0.74	-5.45	-0.84	-3.87	1.58	CN	1.23	-5.94	-0.87	-3.84	1.99
PBCO	0.74	-5.45	-1.10	-3.61	1.84	CO	1.12	-5.83	-1.29	-3.42	2.52
PECN	0.61	-5.32	-0.86	-3.85	1.47	BT	1.84	-6.55	-1.24	-3.47	3.08
PECO	0.44	-5.15	-1.30	-3.41	1.74	NT	2.20	-6.91	-0.74	-3.97	2.94
PNBT	0.68	-5.39	-1.29	-3.42	1.97	TPD	1.95	-6.66	-1.60	-3.11	3.55
PNNT	1.07	-5.78	-0.89	-3.82	1.96	SW	1.76	-6.47	-1.16	-3.55	2.92
PNTPD	0.98	-5.69	-1.47	-3.24	2.45	SF	1.18	-5.89	-0.90	-3.81	2.08
PNSW	0.94	-5.65	-1.34	-3.37	2.28	NDI	1.58	-6.29	-0.75	-3.96	2.33
PNSF	0.96	-5.67	-1.07	-3.64	2.03	PDI	1.63	-6.34	-0.75	-3.96	2.38
PNCN	1.03	-5.74	-0.80	-3.91	1.83	TPTI	1.01	-5.72	-1.76	-2.95	2.77
PNNDI	1.01	-5.72	-0.80	-3.91	1.81						
PNPDI	1.02	-5.73	-0.67	-4.04	1.69						

<sup>a</sup>HOMO levels were determined from the  $E_{onset}$  of the first oxidation potential of ferrocene, -4.8 eV. <sup>b</sup>LUMO levels were determined from the  $E_{onset}$  of the first reduction potential of ferrocene, -4.8 eV. <sup>c</sup>The electrochemical bandgap determined by cyclic voltammetry.

The difference in the LUMO energy levels of those monomers brought a significant effect on the LUMO levels of TPTI-based polymers. LUMO energy levels of these polymers were increased in the following order: PNPDI (-4.04 eV) < PNNDI, PNCN (-3.91 eV) < PNNT (-3.82 eV) < PNSF (-3.64 eV) < PNBT (-3.42 eV) < PNSW (-3.37 eV) < PNTPD (-3.24 eV). As shown in Figure 1, the LUMO



**Figure 1.** The electrochemical bandgap diagram of the monomers and the TPTI-based polymers. The colored lines in the middle column represents the energy levels of the polymers result from copolymerizing TPTI with the corresponding monomers on the right.

energy levels of TPTI-based polymers were determined by those of the electron accepting co-monomers. The strong electron accepting monomers effectively decreased the LUMO energy levels of polymers. All of the TPTI-based polymers exhibited similar HOMO energy levels of -5.65 to -5.78 eV regardless of the difference in electron accepting properties of co-monomers, which are similar to that of the TPTI monomer (-5.72 eV).

The BDT-based polymers also exhibited similar trends with TPTI-based polymers. PBCO and PBCN exhibited identical HOMO energy levels of -5.45 eV, which is also similar to the HOMO energy levels of BDT (-5.51 eV). The LUMO energy levels of PBCN and PBCO are -3.87 and -3.61 eV, respectively, which are similar to the LUMO energy levels of CN (-3.84 eV) and CO (-3.42 eV), respectively. However, in

the case of EDOT-based polymers, the HOMO energy levels of PECN and PECO were significantly decreased to -5.32 and -5.15 eV, respectively, compared to that of EDOT monomer (-4.60 eV). The frontier orbitals of the monomers and the several repeating units of polymers were calculated using the B3LYP function with basis set 6-31G\*, and the results are shown in SI (Figures S11 and S12). The HOMOs of the TPTI-based polymers were highly localized in the amide building block, which means that the HOMOs of the TPTI-based polymers are quite similar to that of the TPTI building block. On the other hands, the LUMOs of the TPTI-based polymers were largely localized in the electron accepting co-monomers. It also indicates that the LUMOs of the TPTI-based polymers resemble those of the stronger electron withdrawing co-monomers. In addition, the LUMOs of polymers containing strong electron accepting co-monomers (PDI, NDI, CN, and SF) have electron density mainly localized on strong electron acceptor units. As a result, those four polymers exhibited almost identical LUMO energy levels with co-monomers. Therefore, the HOMO energy levels of the TPTI-based polymers were determined by a TPTI monomer and the LUMO energy levels by the electron accepting co-monomers.

EDOT-based polymers exhibited similar electron distribution with TPTI-based polymers in LUMOs; electron density is highly withdrawn to the electron accepting moieties; however, in HOMOs, electrons are well-delocalized along the backbone rings. Therefore, the HOMO energy levels of SD-SA-type polymers (PECO and PECN) are determined by both the electron donating and accepting monomers, consistent with experimental results.

**FET Studies and Mobility.** The carrier mobility of the polymers was measured using two types of device structure: FET devices using a top-contact geometry (Figure 2) and sandwich-type devices for SCLC measurements as reported elsewhere.<sup>44</sup> The results are summarized in Table 2. The microstructure of neat polymer films was characterized by using grazing incidence wide-angle X-ray scattering (GIWAXS). Two dimensional (2D) GIWAXS patterns of the neat polymers are shown in Figure 3, and their out-of-plane and in-plane lincuts are shown in the SI (Figure S18). In the FET devices, TPTI-based polymers exhibited much higher electron mobilities than BDT- and EDOT-based polymers. PECO polymer containing strong electron donating EDOT and weak electron accepting CO monomer exhibited only p-type characteristics due to the

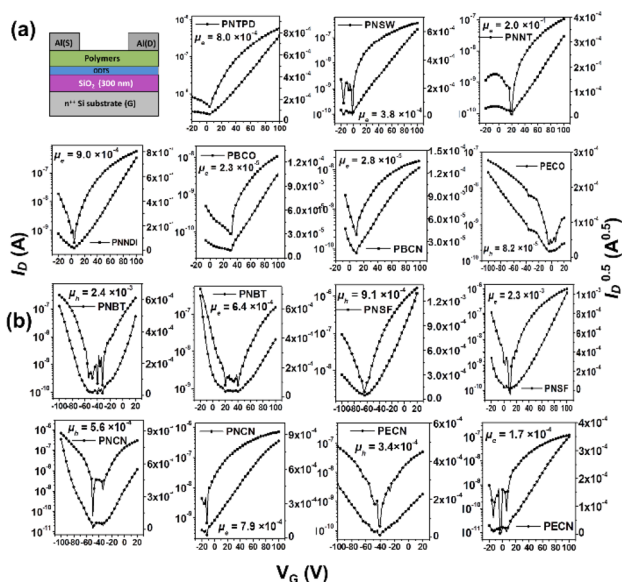


**Figure 2.** Transfer characteristics of the polymers showing (a) unipolar n-type and (b) ambipolar behavior in the saturation regime for FETs fabricated by spin-coating electron accepting polymers on octadecyltrichlorosilane (ODTS)-treated SiO<sub>2</sub>/Si substrates with device structure shown in the top left corner, with the exception of the PECO device utilizing Au as electrodes.

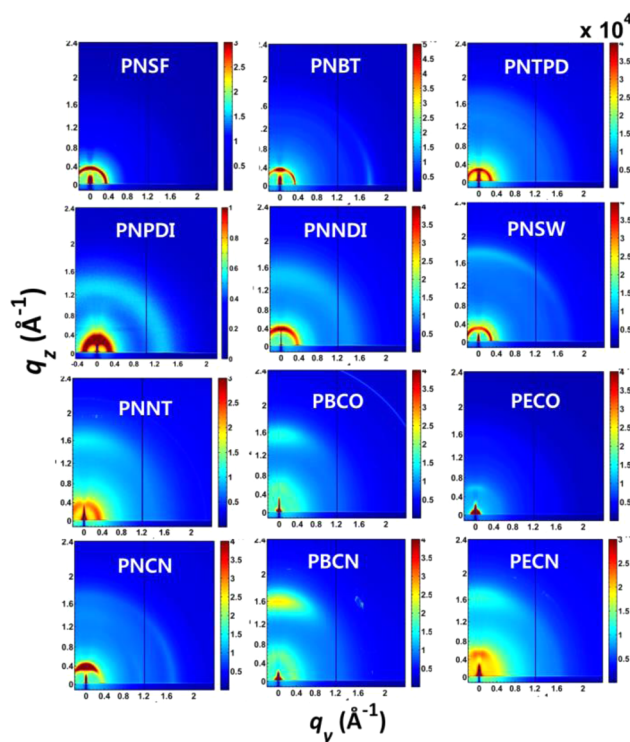


**Figure 3.** 2D GIWAXS patterns for the neat electron accepting polymers.

dominant electron donating properties of EDOT. PNCN, PNSF, PNBT, and PECN exhibited ambipolar field-effect behaviors, and the other polymers showed n-type field-effect characteristics. Among the TPTI-based polymers, PNSF exhibited the highest FET electron mobility of  $2.3 \times 10^{-3} \text{ cm}^2/(\text{V}\cdot\text{s})$  while showing ambipolar behavior with a hole mobility of  $9.1 \times 10^{-4} \text{ cm}^2/(\text{V}\cdot\text{s})$ . The other TPTI-based

polymers exhibited electron mobilities in the range of  $(2-9) \times 10^{-4} \text{ cm}^2/(\text{V}\cdot\text{s})$ .

However, the SCLC electron mobilities of the polymers showed a significantly different trend from those in FET devices. PNBT, PNCN, and PNTPD exhibited FET mobilities of  $(6-8) \times 10^{-4} \text{ cm}^2/(\text{V}\cdot\text{s})$ , but SCLC mobilities of  $(2-5) \times 10^{-5} \text{ cm}^2/(\text{V}\cdot\text{s})$ . On the other hand, PNPDI exhibited a higher SCLC mobility of  $2.7 \times 10^{-4} \text{ cm}^2/(\text{V}\cdot\text{s})$ , but no FET mobility. PNNDI and PNSW showed similar FET and SCLC mobilities of around  $10^{-4} \text{ cm}^2/(\text{V}\cdot\text{s})$ . GIWAXS results indicated that PNBT and PNCN showing the ordering with a *d*-spacing of  $\sim 3.5 \text{ \AA}$  in the edge-on mode exhibited a sizable FET mobility. The polymers exhibiting the face-on orientation of conjugated backbone (PNPDI, PNNDI, and PNSW) showed relatively high SCLC mobilities compared to the other polymers. Since the SCLC devices require a vertical electron transport pathway from the bottom electrode, the ordering toward perpendicular direction should promote electron transport in the SCLC devices. CN-based polymers exhibited higher SCLC mobilities than CO-based polymers due to the better ordering with a *d*-spacing of  $\sim 3.9 \text{ \AA}$  in the face-on mode, as shown in Figure 3.

**Photovoltaic Effect.** To examine the photovoltaic properties of the electron accepting polymers, several materials were used as the electron donor in all-polymer solar cells, namely, PTB7, P3HT, and benzoporphyrin (BP). The BHJ photovoltaic devices were fabricated with the following configuration: ITO/PEDOT:PSS/electron donors:electron accepting polymers/Ca/Al. The photovoltaic characteristics were measured in a glovebox under nitrogen atmosphere. The *J*-*V* characteristics of the devices (under AM 1.5G condition,  $100 \text{ W}/\text{cm}^2$ ) of the PTB7:accepting polymer mixtures are shown in Figure 4a, and

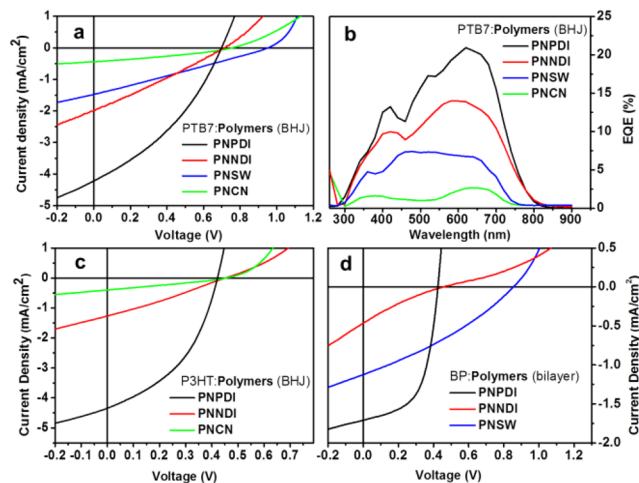


**Figure 4.** (a) *J*-*V* characteristics and (b) external quantum efficiency (EQE) of BHJ photovoltaic devices with an active layer composed of PTB7:electron accepting polymers. *J*-*V* characteristics of (c) P3HT:accepting polymers BHJ devices and (d) BP:polymers bilayer devices under simulated AM 1.5 G solar irradiation.

the corresponding photovoltaic parameters are summarized in Table 4. Detailed studies of the *J*-*V* characteristics as a function of the weight ratio between donor and acceptor are shown in Figure S19 (SI).

Among the synthesized 12 electron accepting polymers, only four polymers exhibited photovoltaic properties. PNPDI exhibited the highest PCE value of 1.03% ( $V_{oc} = 0.69 \text{ V}$ ,  $J_{sc} = -4.13 \text{ mA}/\text{cm}^2$ , and  $\text{FF} = 0.36$ ) at a weight ratio of

Table 4. Summary of Photovoltaic Properties

active layer	device type	$J_{sc}$ (mA/cm <sup>2</sup> )	$V_{oc}$ (V)	fill factor	PCE <sup>a</sup> (PCE <sub>max</sub> ) (%)
PTB7:PNSW (1:1, w/w)	BHJ	-1.46 ± 0.01	0.93 ± 0.02	0.26 ± 0.01	0.35 ± 0.02 (0.37)
BP:PNSW	bilayer	-1.10 ± 0.02	0.86 ± 0.01	0.32 ± 0.003	0.30 ± 0.01 (0.31)
PTB7:PNCN (1:1.5, w/w)	BHJ	-0.42 ± 0.02	0.76 ± 0.01	0.32 ± 0.004	0.10 ± 0.01 (0.11)
P3HT:PNCN (1:1.5, w/w)	BHJ	-0.34 ± 0.06	0.46 ± 0.01	0.29 ± 0.004	0.04 ± 0.01 (0.05)
PTB7:PNNDI (1:1, w/w)	BHJ	-2.28 ± 0.10	0.71 ± 0.01	0.27 ± 0.01	0.43 ± 0.03 (0.46)
P3HT:PNNDI (1:1.5, w/w)	BHJ	-1.19 ± 0.07	0.45 ± 0.01	0.28 ± 0.005	0.15 ± 0.01 (0.16)
BP:PNNDI	bilayer	-0.46 ± 0.01	0.45 ± 0.01	0.20 ± 0.003	0.04 ± 0.01 (0.05)
PTB7:PNPDI (1:1.8, w.w)	BHJ	-4.13 ± 0.09	0.69 ± 0.01	0.36 ± 0.004	1.03 ± 0.03 (1.06)
P3HT:PNPDI (1:1.5, w.w)	BHJ	-4.19 ± 0.14	0.42 ± 0.01	0.43 ± 0.005	0.75 ± 0.04 (0.79)
BP:PNPDI	bilayer	-1.63 ± 0.08	0.43 ± 0.01	0.57 ± 0.004	0.40 ± 0.01 (0.41)

<sup>a</sup>Average value from four to eight devices.

PTB7:PNPDI = 1:1.8. PNNDI and PNSW showed PCE of 0.43% ( $V_{oc}$  = 0.71 V,  $J_{sc}$  = -2.28 mA/cm<sup>2</sup>, and FF = 0.27) and 0.35% ( $V_{oc}$  = 0.93 V,  $J_{sc}$  = -1.46 mA/cm<sup>2</sup>, and FF = 0.26), respectively, at a weight ratio of PTB7:PNNDI or PNSW = 1:1. Lastly, PNCN exhibited the lowest PCE value of 0.10% ( $V_{oc}$  = 0.76 V,  $J_{sc}$  = -0.42 mA/cm<sup>2</sup>, and FF = 0.32) at a weight ratio of PTB7:PNCN = 1:1.5. The external quantum efficiency (EQE) curves of PTB7:accepting polymer devices are shown in Figure 4b, which are in good agreement with the  $J_{sc}$  values. The open circuit voltage is linearly dependent on the HOMO level of the donor (p-type semiconductor quasi Fermi level) and the LUMO level of the acceptor (n-type semiconductor quasi Fermi level).<sup>45</sup> As a result, the  $V_{oc}$  was increased in the order of PNPDI (-4.04 eV) < PNNDI (-3.91 eV) < PNCN (-3.91 eV) < PNSW (-3.37 eV). However, all of the solar cells exhibited relatively small fill factors, less than 0.36. In general, fill factor is determined by the series resistance ( $R_s$ ), shunt resistance ( $R_{sh}$ ), and diode parameters ( $n$  and  $J_s$ ), all of which are the function of charge carrier mobility.<sup>46</sup> The dominating contribution to the  $R_s$  is the large resistivity of the organic layers. Space charge formation and bimolecular recombination from the carrier with low mobility induce charge carriers' loss and increase in  $R_{sh}$ .<sup>47</sup> Therefore, both cases require the high mobility of the electron accepting polymers to improve the FF in the photovoltaic devices. When P3HT was used as an electron donor, the  $V_{oc}$  of the devices was significantly decreased due to the higher HOMO energy level (~5.0 eV) of P3HT than that of PTB7 (-5.3 eV). Interestingly, thermal annealing P3HT:PNPDI device resulted in higher FF and  $J_{sc}$  values than PTB7:PNPDI devices. It is likely that the annealing process enhanced the ordering of P3HT in the blended films, which facilitated the formation of a nanoscale interpenetrating network between donor and acceptor, enhancing charge transport. We have also fabricated the bilayer devices using BP as the electron donor. The donor layer was formed by solution process from a soluble precursor, tetraethanotetra-benzoporphyrin (CP), and then thermally converted in the insoluble semiconducting BP film. BP:PNPDI bilayer device exhibited a highest FF value of 0.57 compared to the other devices. It is expected that the nongeminate (bimolecular) recombination in the bilayer devices are minimized compared to that in the BHJ devices, because the hole (or electron) already transported to the electron donor (or acceptor) cannot recombine with electron (or hole).<sup>48,49</sup> BP:PNSW bilayer devices also exhibited a higher FF than PTB7:PNSW BHJ devices similar to PNPDI devices. However, the bilayer devices exhibited lower  $J_{sc}$  values than BHJ devices due to the limited interfacial area between electron donor and acceptor.

The electron accepting polymers exhibiting a SCLC mobility less than 10<sup>-4</sup> cm<sup>2</sup>/(V·s) did not exhibit any noticeable photovoltaic performance when they were combined with PTB7 that exhibits a hole mobility of ~10<sup>-3</sup> cm<sup>2</sup>/(V·s). The polymers showing SCLC mobilities higher than 10<sup>-4</sup> cm<sup>2</sup>/(V·s) exhibited photovoltaic properties. There is no clear relationship between the FET mobility and the photovoltaic performance. It can be expected that if the electron mobilities of the accepting polymers are increased to or above the level of ~10<sup>-3</sup> cm<sup>2</sup>/(V·s), well-balanced with that of electron donor materials, much higher FF and  $J_{sc}$  values in photovoltaic devices can be achieved by reducing the charge recombination and space charge formation as well as increasing exciton dissociation and carrier transport.

## DISCUSSION

**Determination of HOMO and LUMO Levels of Electron Accepting Polymers.** Among the four polymer repeating structures, (a) WD-SA (PBCN and PBCO), (b) WA-SA (PNPDI, PNNDI, PNCN, PNSF, and PNNT), (c) WA-WA (PNTPD, PNSW, and PNBt), (d) SD-SA (PECN and PECO), the SA determines the LUMO energy levels of the polymers. The HOMO energy levels of those polymers with WA-SA (e.g., the TPTI-based polymers) and WD-SA (e.g., the BDT-based polymers) are mainly determined by WA and WD, respectively. Both the theoretical simulation of the frontier orbitals of polymers and electrochemical studies support the conclusion. The polymers with the WD-SA (PBCO and PBCN) structure exhibit rather low-lying LUMO energy levels, but their HOMO energy levels are too high due to the high-lying HOMO energy level of the BDT monomer (WD), and the electron mobilities are relatively poor.

An interesting observation of the consequence of low LUMO energy levels is the relationship between LUMO energy levels and fluorescence quantum yields (QYs) of the polymers containing TPTI. The fluorescence QY of the polymers was quantified in a diluted solution; the intensity at the absorption maxima was kept at 0.03 to prevent the aggregation effect. Fluorescein was used as a reference fluorescence dye, whose QY in ethanol is known to be 0.79.<sup>50</sup> The QYs of the polymers as listed in Table 2 are significantly changed depending on the electron accepting moiety. The QYs of the polymers are nonlinearly reduced as the LUMO energy levels of polymers are decreased (Figure 5). Since the LUMO energy levels of TPTI-based polymers are highly related with the electron withdrawing properties of the co-monomers, it is expected that the stronger electron accepting co-monomers quenched the PL emission of the polymers more effectively due to internal

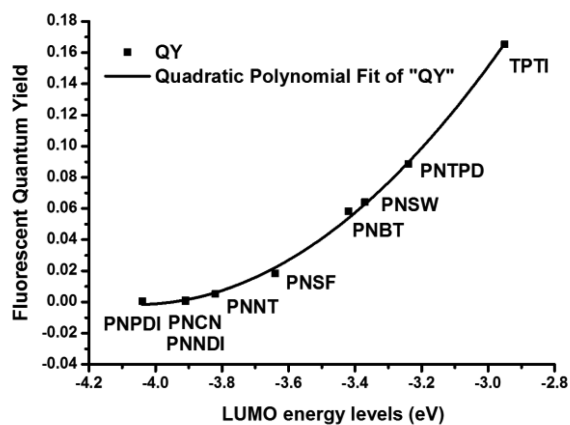


Figure 5. Fluorescent quantum yield (QY) vs LUMO levels of the TPTI-based polymers.

polarization. Both LUMO and HOMO energy levels in accepting polymers should be sufficiently low enough to enhance the driving force for charge separation from a donor polymer to an accepting polymer. In addition, the internal polarization between the two monomers is also beneficial to charge separation. Indeed, PNPDI and PNNDI having LUMO energy levels of  $-4.04$  and  $-3.91$  eV, respectively, exhibited higher  $J_{sc}$  values than the other polymers.

Interestingly, the polymers containing a strong electron accepting CN moiety did not exhibit any emission in film states. In solution, CN-based polymers also exhibited the worst QYs in the series of polymers. However, PNCN having deep LUMO levels of  $-3.91$  eV showed a significantly poor  $J_{sc}$  value in the photovoltaic devices. The difference from other accepting monomers is that CN monomer has the two dicyanovinylene moieties functionalized in the same direction of the conjugated backbone, which can generate large polarization between the ground and excited states. Therefore, the dicyanovinylene moieties can act as electron trapping sites. In addition, the dicyanovinyl groups orthogonally attached to the conjugated backbone can lead to localized LUMOs and low fluorescent QYs of the CN-based polymers.<sup>38</sup> Indeed, CN-based polymers exhibited poor SCLC electron mobilities in the range of  $10^{-5}$ – $10^{-6}$   $\text{cm}^2/(\text{V}\cdot\text{s})$  compared with those of PNPDI and PNNDI even though CN-based polymers are more planar and exhibited very small dihedral angles and strong preference to the face-on orientation.

## CONCLUSION

We have developed new electron-deficient TPTI and CN monomers and synthesized a series of alternating electron accepting polymers containing different monomer combinations: (a) WD-SA, (b) WA-SA, (c) WA-WA, and (d) SD-SA. It was found that LUMO energy levels of the electron accepting polymers are significantly determined by those of stronger electron accepting monomers and the HOMOs are largely decided by the weak accepting (or weak donating) monomers. Fluorescent measurements indicated that the QYs of the TPTI-based polymers are nonlinearly reduced as the LUMO energy levels of polymers are decreased, which has a close relationship with PCE of photovoltaic cells, implying internal polarization is important for photovoltaic application. To control the energy levels of both HOMO and LUMO and at the same time introduce internal polarization, polymers with WA-SA structures were found to be desirable. It was found that the

SCLC mobility plays a much more important role than FET mobility for determining the photovoltaic performance. Overall, this work offers a new outlook for developing better electron accepting materials by providing an in-depth study of structure–property relationships.

## EXPERIMENTAL SECTION

**Materials.** 1,3-Dibromo-5-(2-ethylhexyl)-4H-thieno[3,4-c]pyrrole-4,6(5H)-dione (TPD),<sup>51</sup> 1,3-dibromo-5-(2-ethylhexyl)thieno[3,4-d]-isothiazol-3(2H)one-1,1-dioxide (SW),<sup>52</sup> 4,7-dibromobenzo[*c*][1,2,5]-thiadiazole (BT),<sup>53</sup> 2,5-dibromo-3,4-dinitrothiophene (NT),<sup>54</sup> 2,6-bis(trimethyltin)-4,8-bis(2-ethylhexyloxy)benzo[1,2-*b*:4,5-*b'*]-dithiophene (BDT),<sup>55</sup> 5,7-bis(trimethylstannyl)-2,3-dihydrothieno[3,4-*b*][1,4]dioxine (EDOT),<sup>56</sup> 4,9-dibromo-2,7-bis(2-ethylhexyl)-benzo[*lmn*][3,8]-phenanthroline-1,3,6,8(2H,7H)-tetraone (NDI),<sup>57</sup> and *N,N'*-bis(2-decyltetradecyl)-1,7-dibromo-3,4,9,10-perylene diimide (PDI),<sup>58</sup> were synthesized according to literature procedures, and their structural characterization through the MALDI-TOF mass and NMR spectroscopy was described in the SI. All of the chemicals were purchased from Aldrich except for tetrakis(triphenylphosphine) palladium from Strem Chemicals. All reagents purchased commercially were used without further purification except for toluene and tetrahydrofuran (THF), which were dried over sodium–benzophenone. <sup>1</sup>H NMR and <sup>13</sup>C NMR spectra were recorded on a Bruker DRX-400 spectrometer, with tetramethylsilane as an internal reference. Matrix-assisted laser desorption ionization time-of-flight (MALDI-TOF) mass spectra were recorded using a Bruker Ultraflexreme MALDI-TOF/TOF mass spectrometer with dithranol as the matrix. Elemental analysis was performed by Midwest MicroLab. The number- and weight-average molecular weights of the polymers were determined by gel-permeation chromatography (GPC) with a Waters Associates liquid chromatography instrument equipped with a Waters 510 HPLC pump, a Waters 410 differential refractometer, and a Waters 486 tunable absorbance detector. THF was used as the eluent and polystyrene as the standard. TGA measurement of the polymers was performed using a TA Q600 instrument. UV–vis absorption spectra were measured on a Shimadzu UV-3600 device. Cyclic voltammetry was performed on an AUTOLAB/PG-STAT12 model system with a three-electrode cell in a 0.1 N Bu<sub>4</sub>NBF<sub>4</sub> solution in acetonitrile at a scan rate of 50 mV/s. A film of each polymer was coated onto a Pt wire electrode by dipping the electrode into a polymer solution in chloroform. All measurements were calibrated against an internal standard of ferrocene (Fc), the ionization potential (IP) value of which is  $-4.8$  eV for the Fc/Fc<sup>+</sup> redox system. AFM images were obtained by using an Asylum MFP-3D microscope. TEM measurements were performed by using a Tecnai F-30 with an accelerating voltage at 300 kV.

**PSC Device Fabrication.** Polymeric solar cells with a device configuration of glass/indium tin oxide (ITO)/poly(3,4-ethylenedioxythiophene):poly(styrenesulfonate) (PEDOT:PSS)/PTB7, P3HT or BP:accepting polymers/Ca/Al were prepared. Prior to device fabrication, the ITO substrates were cleaned with detergent and ultrasonicated in deionized water, acetone, and isopropanol and then dried overnight in an oven. The substrate was spin-coated by a PEDOT:PSS solution and dried at 100 °C in N<sub>2</sub> for 30 min, and then transferred to a glovebox for spin-casting of the polymer layer. The solution (chloroform:1,8-diiodooctane = 98:2 (v/v)) containing a blended mixture of PTB7/accepting polymers was spin-casted by 6000 rpm, onto the above substrate. PTB7/acceptor films were used directly without annealing process. The solution (chloroform:*p*-xylene = 3:2 (v/v)) of P3HT/accepting polymers was spin-coated by 2800 rpm and annealed at 150 °C for 30 min. In case of bilayer devices, a soluble precursor, tetraethanotetrabenzoporphyrin (CP) in chloroform (1.0 wt %) was spin-coated by 1500 rpm and then thermally converted in the insoluble semiconducting BP film at 180 °C for 10 min. Onto the BP substrate, the electron accepting polymer in chloroform (0.8 wt %) was spin-casted by 2800 rpm. Subsequently, the device was pumped down under vacuum ( $<10^{-6}$  Torr) and the Ca (20 nm) and Al (80 nm) electrode was deposited by thermal evaporation

in the glovebox at a chamber pressure of  $\sim 5.0 \times 10^{-7}$  Torr. The active area of the solar cell is  $3.14 \text{ mm}^2$ , which is defined by the cathode area. Current density–voltage ( $J$ – $V$ ) characteristics of the devices under nitrogen were measured using a Keithley 238 Source Measure unit. The photovoltaic properties were characterized under an Air Mass 1.5 Global (AM 1.5G) solar simulator with irradiation intensity of  $100 \text{ mW/cm}^2$ .

**FET Device Fabrication.** Heavily doped Si substrates coated with thermally grown  $300 \text{ nm SiO}_2$  were used as gate substrates (Silicon Inc.). The substrate was cleaned by piranha treatment followed by multiple rinsing with DI water, and then treated with octadecyltrichlorosilane (ODTS).  $0.2$ – $0.3 \text{ wt } \%$  solutions of the polymers (in chloroform) were spin-coated on the ODTS-treated Si substrates. The polymer films were annealed at  $180 \text{ }^\circ\text{C}$  for  $10 \text{ min}$  to improve their crystallinity. To complete top-contact polymer FET devices, Al was thermally evaporated through a shadow mask, which forms  $100 \text{ nm}$  thick source/drain electrodes (channel length/width ( $W/L$ ) =  $50 \text{ }\mu\text{m}/(1500 \text{ }\mu\text{m})$ ). FET transfer characteristics were measured in the saturation regime, and the FET mobility was calculated using the following equation by fitting experimental values:  $I_D = \mu C_i W(2L)^{-1}(V_G - V_{Th})^2$ , where  $C_i$  and  $V_{Th}$  are the capacitance per unit area of the gate dielectrics and the threshold voltage, respectively. All of the fabrication steps and electrical measurements were performed in a  $\text{N}_2$ -filled glovebox ( $\text{O}_2/\text{H}_2\text{O} < 0.1 \text{ ppm}$ )

## ■ ASSOCIATED CONTENT

### ■ Supporting Information

Scheme showing synthesis of monomers, text describing the syntheses, general procedure for polymerization, and mobility measurements, figures showing NMR spectra of compounds **6**, **7**, **13**, **14**, NDI, EDOT, SW, and TDP, MALDI-TOF mass spectra of compounds **6**, **7**, **13**, and **14**, TGA thermograms of polymers, HOMO and LUMO diagrams of the four polymer repeating units and of the monomers, HOMO and LUMO energy level diagrams, absorption, cyclic voltammograms of the monomers, linecuts of neat electron accepting polymers, plots of  $J$ – $V$  characteristics, and AFM images, and a table listing electrochemical properties of select polymers. This material is available free of charge via the Internet at <http://pubs.acs.org>.

## ■ AUTHOR INFORMATION

### Corresponding Author

\*E-mail: lupingyu@uchicago.edu.

### Notes

The authors declare no competing financial interest.

## ■ ACKNOWLEDGMENTS

This work is supported by a U.S. National Science Foundation Grant (NSF DMR-1263006), the Air Force Office of Scientific Research and NSF MRSEC program at the University of Chicago (Grant DMR-0213745), Department of Energy (DOE) via the ANSER Center, an Energy Frontier Research Center funded by the U.S. Department of Energy, Office of Science, Office of Basic Energy Sciences, under Award No. DE-SC0001059. W.C. gratefully acknowledges financial support from the U.S. Department of Energy, Office of Science, Office of Basic Energy Sciences, under Award No. KC020301. We also thank Dr. Joseph Strzalka and Dr. Zhang Jiang for the assistance with GISAXS measurements. Use of the Advanced Photon Source (APS) at Argonne National Laboratory was supported by the U.S. Department of Energy, Office of Science, Office of Basic Energy Sciences, under Contract No. DE-AC02-06CH11357.

## ■ REFERENCES

- (1) Brabec, C. J.; Sariciftci, N. S.; Hummelen, J. C. *Adv. Funct. Mater.* **2001**, *11*, 15.
- (2) Coakley, K. M.; McGehee, M. D. *Chem. Mater.* **2004**, *16*, 4533.
- (3) Kraabel, B.; Lee, C. H.; McBranch, D.; Moses, D.; Sariciftci, N. S.; Heeger, A. J. *Chem. Phys. Lett.* **1993**, *213*, 389.
- (4) Yu, G.; Gao, J.; Hummelen, J. C.; Wudl, F.; Heeger, A. J. *Science* **1995**, *270*, 1789.
- (5) Halls, J. J. M.; Walsh, C. A.; Greenham, N. C.; Marseglia, E. A.; Friend, R. H.; Moratti, S. C.; Holmes, A. B. *Nature* **1995**, *376*, 498.
- (6) Granstrom, M.; Petritsch, K.; Arias, A. C.; Lux, A.; Andersson, M. R.; Friend, R. H. *Nature* **1998**, *395*, 257.
- (7) Kim, Y.; Cook, S.; Choulis, S. A.; Nelson, J.; Durrant, J. R.; Bradley, D. D. C. *Chem. Mater.* **2004**, *16*, 4812.
- (8) Alam, M. M.; Jenekhe, S. A. *Chem. Mater.* **2004**, *16*, 4647.
- (9) Zhan, X.; Tan, Z.; Domercq, B.; An, Z.; Zhang, X.; Barlow, S.; Li, Y.; Zhu, D.; Kippelen, B.; Marder, S. R. *J. Am. Chem. Soc.* **2007**, *129*, 7246.
- (10) Liang, Y.; Xu, Z.; Xia, J.; Tsai, S.-T.; Wu, Y.; Li, G.; Ray, C.; Yu, L. *Adv. Mater.* **2010**, *22*, E135.
- (11) Park, S. H.; Roy, A.; Beaupre, S.; Cho, S.; Coates, N.; Moon, J. S.; Moses, D.; Leclerc, M.; Lee, K.; Heeger, A. J. *Nat. Photonics* **2009**, *3*, 297.
- (12) Dou, L.; You, J.; Yang, J.; Chen, C.-C.; He, Y.; Murase, S.; Moriarty, T.; Emery, K.; Li, G.; Yang, Y. *Nat. Photonics* **2012**, *6*, 180.
- (13) Zhou, N.; Guo, X.; Ortiz, R. P.; Li, S.; Zhang, S.; Chang, R. P. H.; Facchetti, A.; Marks, T. J. *Adv. Mater.* **2012**, *24*, 2242.
- (14) Small, C. E.; Chen, S.; Subbiah, J.; Amb, C. M.; Tsang, S.-W.; Lai, T.-H.; Reynolds, J. R.; So, F. *Nat. Photonics* **2012**, *6*, 115.
- (15) Meager, I.; Ashraf, R. S.; Mollinger, S.; Schroeder, B. C.; Bronstein, H.; Beatrup, D.; Vezie, M. S.; Kirchartz, T.; Salleo, A.; Nelson, J.; McCulloch, I. *J. Am. Chem. Soc.* **2013**, *135*, 11537.
- (16) Lei, T.; Dou, J.-H.; Cao, X.-Y.; Wang, J.-Y.; Pei, J. *J. Am. Chem. Soc.* **2013**, *135*, 12168.
- (17) Yuen, J. D.; Fan, J.; Seifert, J.; Lim, B.; Hufschmid, R.; Heeger, A. J.; Wudl, F. *J. Am. Chem. Soc.* **2011**, *133*, 20799.
- (18) Zhan, X.; Facchetti, A.; Barlow, S.; Marks, T. J.; Ratner, M. A.; Wasielewski, M. R.; Marder, S. R. *Adv. Mater.* **2011**, *23*, 268.
- (19) Nielsen, C. B.; Turbiez, M.; McCulloch, I. *Adv. Mater.* **2013**, *25*, 1859.
- (20) Lei, T.; Dou, J.-H.; Cao, X.-Y.; Wang, J.-Y.; Pei, J. *Adv. Mater.* **2013**, *25*, 6589.
- (21) Lei, T.; Xia, X.; Wang, J.-Y.; Liu, C.-J.; Pei, J. *J. Am. Chem. Soc.* **2014**, *136*, 2135.
- (22) Li, H.; Kim, F. S.; Ren, G.; Jenekhe, S. A. *J. Am. Chem. Soc.* **2013**, *135*, 14920.
- (23) Earmme, T.; Hwang, Y.-J.; Murari, N. M.; Subramaniyan, S.; Jenekhe, S. A. *J. Am. Chem. Soc.* **2013**, *135*, 14960.
- (24) Zhou, E.; Cong, J.; Hashimoto, K.; Tajima, K. *Adv. Mater.* **2013**, *25*, 6991.
- (25) Cao, Y.; Lei, T.; Yuan, J.; Wang, J.-Y.; Pei, J. *Polym. Chem.* **2013**, *4*, 5228.
- (26) Cheng, P.; Ye, L.; Zhao, X.; Hou, J.; Li, Y.; Zhan, X. *Energy Environ. Sci.* **2014**, *7*, 1351.
- (27) Yan, H.; Chen, Z.; Zheng, Y.; Newman, C.; Quinn, J. R.; Dotz, F.; Kastler, M.; Facchetti, A. *Nature* **2009**, *457*, 679.
- (28) Zhou, N.; Lin, H.; Lou, S. J.; Yu, X.; Guo, P.; Manley, E. F.; Loser, S.; Hartnett, P.; Huang, H.; Wasielewski, M. R.; Chen, L. X.; Chang, R. P. H.; Facchetti, A.; Marks, T. J. *Adv. Energy Mater.* **2014**, *4*, 1300785.
- (29) Mori, D.; Benten, H.; Okada, I.; Ohkita, H.; Ito, S. *Adv. Energy Mater.* **2014**, *4*, 1301006.
- (30) Steyrleuthner, R.; Schubert, M.; Jaiser, F.; Blakesley, J. C.; Chen, Z.; Facchetti, A.; Neher, D. *Adv. Mater.* **2010**, *22*, 2799.
- (31) Li, W.; Roelofs, W. S. C.; Turbiez, M.; Wienk, M. M.; Janssen, R. A. J. *Adv. Mater.* **2014**, DOI: 10.1002/adma.201305910.
- (32) Facchetti, A. *Mater. Today* **2013**, *16*, 123.
- (33) Marcus, R. A. *J. Chem. Phys.* **1956**, *24*, 966.
- (34) Piotrowiak, P. *Chem. Soc. Rev.* **1999**, *28*, 143.

- (35) Hoppe, H.; Niggemann, M.; Winder, C.; Kraut, J.; Hiesgen, R.; Hinsch, A.; Meissner, D.; Sariciftci, N. S. *Adv. Funct. Mater.* **2004**, *14*, 1005.
- (36) Cao, J.; Liao, Q.; Du, X.; Chen, J.; Xiao, Z.; Zuo, Q.; Ding, L. *Energy Environ. Sci.* **2013**, *6*, 3224.
- (37) Wu, J.-S.; Cheng, Y.-J.; Dubosc, M.; Hsieh, C.-H.; Chang, C.-Y.; Hsu, C.-S. *Chem. Commun. (Cambridge, U. K.)* **2010**, *46*, 3259.
- (38) Grimm, B.; Risko, C.; Azoulay, J. D.; Bredas, J.-L.; Bazan, G. C. *Chem. Sci.* **2013**, *4*, 1807.
- (39) Lee, C.; Yang, W.; Parr, R. G. *Phys. Rev. B* **1988**, *37*, 785.
- (40) Tirado-Rives, J.; Jorgensen, W. L. *J. Chem. Theory Comput.* **2008**, *4*, 297.
- (41) Brédas, J. L.; Street, G. B.; Thémans, B.; André, J. M. *J. Chem. Phys.* **1985**, *83*, 1323.
- (42) Pommerehne, J.; Vestweber, H.; Guss, W.; Mahrt, R. F.; Bässler, H.; Porsch, M.; Daub, J. *Adv. Mater.* **1995**, *7*, 551.
- (43) Ruoff, R. S.; Kadish, K. M.; Bouldas, P.; Chen, E. C. M. *J. Phys. Chem.* **1995**, *99*, 8843.
- (44) Mihailitchi, V. D.; van Duren, J. K. J.; Blom, P. W. M.; Hummelen, J. C.; Janssen, R. A. J.; Kroon, J. M.; Rispen, M. T.; Verhees, W. J. H.; Wienk, M. M. *Adv. Funct. Mater.* **2003**, *13*, 43.
- (45) Brabec, C. J.; Cravino, A.; Meissner, D.; Sariciftci, N. S.; Fromherz, T.; Rispen, M. T.; Sanchez, L.; Hummelen, J. C. *Adv. Funct. Mater.* **2001**, *11*, 374.
- (46) Green, M. A. *Sol. Cells* **1982**, *7*, 337.
- (47) Qi, B.; Wang, J. *Phys. Chem. Chem. Phys.* **2013**, *15*, 8972.
- (48) Liu, Y.; Chen, C.-C.; Hong, Z.; Gao, J.; Yang, Y.; Zhou, H.; Dou, L.; Li, G. *Sci. Rep.* **2013**, DOI: 10.1038/srep03356.
- (49) Mauer, R.; Howard, I. A.; Laquai, F. *J. Phys. Chem. Lett.* **2010**, *1*, 3500.
- (50) Kellogg, R. E.; Bennett, R. G. *J. Chem. Phys.* **1964**, *41*, 3042.
- (51) Piliago, C.; Holcombe, T. W.; Douglas, J. D.; Woo, C. H.; Beaujuge, P. M.; Fréchet, J. M. J. *J. Am. Chem. Soc.* **2010**, *132*, 7595.
- (52) Abou-Gharbia, M.; Moyer, J. A.; Patel, U.; Webb, M.; Schiehser, G.; Andree, T.; Haskins, J. T. *J. Med. Chem.* **1989**, *32*, 1024.
- (53) Pilgram, K.; Zupan, M.; Skiles, R. J. *Heterocycl. Chem.* **1970**, *7*, 629.
- (54) Zhang, Q. T.; Tour, J. M. *J. Am. Chem. Soc.* **1998**, *120*, 5355.
- (55) Liang, Y.; Feng, D.; Wu, Y.; Tsai, S.-T.; Li, G.; Ray, C.; Yu, L. *J. Am. Chem. Soc.* **2009**, *131*, 7792.
- (56) Apperloo, J. J.; Groenendaal, L. B.; Verheyen, H.; Jayakannan, M.; Janssen, R. A. J.; Dkhissi, A.; Beljonne, D.; Lazzaroni, R.; Brédas, J.-L. *Chem.—Euro. J.* **2002**, *8*, 2384.
- (57) Guo, X.; Watson, M. D. *Org. Lett.* **2008**, *10*, 5333.
- (58) Rajasingh, P.; Cohen, R.; Shirman, E.; Shimon, L. J. W.; Rybtchinski, B. *J. Org. Chem.* **2007**, *72*, 5973.